

## Electronic Supplementary Information

### Regulation of Double Luminescent Centers Based on the Evolution of Disordered Local Structure for Ratiometric Temperature Sensing Application

*Ting Yu, Bochen Liu, Zhe Ma, Yingyi Jiang, Qingguang Zeng, Dawei Wen\*, Yue Guo\**

School of Applied Physics and Materials, Wuyi University, Jiangmen, Guangdong,  
529020, P. R. China

E-mail: [ontaii@163.com](mailto:ontaii@163.com), [guoyuewuyi@163.com](mailto:guoyuewuyi@163.com)

#### Details of calculation

First-principles DFT calculations were conducted using the Vienna *ab initio* simulation package (VASP) 6.1.<sup>[1]</sup> The generalized gradient approximation of Perdew, Burke, and Ernzerhof (PBE-GGA) with the projector-augmented-wave function (PAW) was applied. The lattice parameters and atomic coordinates were optimized by the conjugate gradient algorithm using VASP 6.1. Due to the cation-disordering nature of  $\text{Sr}_3\text{La}(\text{PO}_4)_3$ , the model construction will break the cubic symmetry of the origin lattice. Thus, the cell parameters were fixed based on the Rietveld refinement results in the structural optimization, leaving the atomic positions relaxable. The modeling is described in Figure S6. The convergence criteria of total energy and residual atomic forces were set to  $10^{-8}$  eV per unit cell and  $2 \times 10^{-2}$  eV/Å, respectively. A mesh of  $2 \times 2 \times 2$  K-points is used. The Sr  $4s^2 4p^6 5s^2$ , La  $5s^2 5p^6 5d^1 6s^2$ , Eu  $5p^6 6s^2$ , P

3s<sup>2</sup>3p<sup>3</sup>, and O 2s<sup>2</sup>2p<sup>4</sup> electrons were treated as valence electrons. The optical and magnetic properties of Eu is not analyzed through DFT this time. Therefore, we chose the Eu\_2 (5p<sup>6</sup>6s<sup>2</sup>) pseudopotential provided by VASP program.

The Debye temperature  $\Theta_D$  was calculated based on the harmonic Debye model, relying on the bulk modulus and Poisson ratio:<sup>[2]</sup>

$$\Theta_D = \frac{\hbar}{k_B} [6\pi^2 V^{1/2} N]^{1/3} \sqrt{\frac{B_H}{M}} f(\nu)$$

where  $\hbar$  is the Plank constant,  $k_B$  is the Boltzmann constant,  $M$  is the molecular mass of the unit cell,  $N$  is the number of atoms in the unit cell,  $B_H$  is the bulk modulus of the crystal,  $V$  is the unit cell volume, and  $f(\nu)$  is

$$f(\nu) = \left\{ 3 \left[ 2 \left( \frac{2}{3} \times \frac{1+\nu}{1-2\nu} \right)^{3/2} + \left( \frac{1}{3} \times \frac{1+\nu}{1-\nu} \right)^{3/2} \right] - 1 \right\}^{1/3}$$

where  $\nu$  is the Poisson ratio. The elastic moduli, including  $B_H$ ,  $G_H$  (shear modulus), and  $\nu$  were be calculated using Voigt–Reuss–Hill (VRH) approximations based on the elastic constants ( $C_{ij}$ ) determined by VASP 6.1.<sup>[3]</sup>

The potential energy barrier from O1 to O2 positions was calculated by the Nudged Elastic Band method with climbing image modification.<sup>[4]</sup> Three images for transition states were inserted between the initial and final states to search the saddle point. The possibility of O1 to O2 vibration was further calculated via the band valence energy landscape analysis, using the output model of Rietveld refinement.<sup>[5]</sup>

**Table S1.** Rietveld refinement result of Sr<sub>2.98</sub>Eu<sub>0.01</sub>La<sub>1.01</sub>P<sub>2.99</sub>Si<sub>0.01</sub>O<sub>12</sub>.

---

$R_{wp} = 7.455\%$ ;  $R_p = 5.887\%$ ;  $S = 1.3516$

Space Group:  $I\bar{4}3d$  (NO.220)

$a = 10.18576(28)$

---

<i>Site</i>	<i>Occ</i>	<i>x</i>	<i>y</i>	<i>z</i>	<i>B</i> <sub>iso</sub>
Sr/La/Eu	0.745/0.252/0.003	0.0624(2)	0.0624	0.0624	1.399(54)
P/Si	0.997/0.003	0.375	0	0.25	1.279(276)
O1	0.4125(115)	0.438(3)	0.382(3)	0.733(4)	0.6*
O2	0.5875	0.5738(14)	0.3492(12)	0.696(3)	0.6*

---

\*The atomic displacement parameters of oxygen were fixed owing to the relatively low charge density and high uncertainty.

**Table S2.** Rietveld refinement result of  $\text{Sr}_{2.69}\text{Eu}_{0.01}\text{La}_{1.30}\text{P}_{2.70}\text{Si}_{0.30}\text{O}_{12}$ .

---

$R_{wp} = 7.612\%$ ;  $R_p = 6.044\%$ ;  $S = 1.3847$

Space Group:  $I\bar{4}3d$  (NO.220)

$a = 10.18735(29)$

---

<i>Site</i>	<i>Occ</i>	<i>x</i>	<i>y</i>	<i>z</i>	<i>B</i> <sub>iso</sub>
Sr/La/Eu	0.673/0.325/0.003	0.0625(2)	0.0625	0.0625	1.490(52)
P/Si	0.900/0.100	0.375	0	0.25	2.067(320)
O1	0.3914(115)	0.436(3)	0.383(3)	0.729(4)	0.6*
O2	0.6086	0.5707(14)	0.3505(12)	0.696(3)	0.6*

---

\*The atomic displacement parameters of oxygen were fixed owing to the relatively low charge density and high uncertainty.

**Table S3.** The bond length of Eu-O1 and Eu-O2

	Eu-O1 (Å)	Eu-O2 (Å)
	2.3862	2.38153
	2.42394	2.42493
	2.52297	2.48018
	2.60329	2.49376
	2.62116	2.58033
	2.79258	2.60991
	2.85903	2.74802
	2.88533	3.05269
	2.91299	
Average	2.6675	2.5964

Cut off distance: 3.5 Å.

**Table S4.** The fitted B、 C and E values of  $\text{Sr}_{2.99-x}\text{Eu}_{0.01}\text{La}_{1+x}\text{P}_{3-x}\text{Si}_x\text{O}_{12}$ .

<b>Fitted results</b>	<b><math>x = 0.05</math></b>	<b><math>x = 0.10</math></b>	<b><math>x = 0.20</math></b>	<b><math>x = 0.30</math></b>
<b>B</b>	0.4925	0.3371	0.2641	0.1274
<b>C</b>	71.643	374.15	369.34	498.91
<b>E</b>	0.1374	0.1874	0.2218	0.2529
<b>Adj. R-Square</b>	0.9993	0.9979	0.9994	0.9981

**Table S5.** Summarized thermometric behaviors of luminescent compounds doped with rare-earth ions.

Luminescent compounds	$\lambda_{\text{ex}}(\text{nm})$	Temperature(K)	$S_r$	References
<b>LaMg<sub>0.402</sub>Nb<sub>0.598</sub>O<sub>3</sub>:Pr<sup>3+</sup></b>	450	298-523	0.725% K <sup>-1</sup>	6
<b>NaLaMgWO<sub>6</sub>:Er<sup>3+</sup></b>	377.75	303-483	1.04% K <sup>-1</sup>	7
<b>YF<sub>3</sub>:Pr<sup>3+</sup></b>	457	293-421	1.24% K <sup>-1</sup>	8
<b>BaTiO<sub>3</sub>: 0.01%Pr<sup>3+</sup>, 8%Yb<sup>3+</sup></b>	980	313-500	1.23% K <sup>-1</sup>	9
<b>LiYO<sub>2</sub>:Pr<sup>3+</sup></b>	280	329	23.04% K <sup>-1</sup>	10
<b>Sr<sub>2.99-x</sub>Eu<sub>0.01</sub>La<sub>1+x</sub>P<sub>3-x</sub>Si<sub>x</sub>O<sub>12</sub></b>	362	303-533	$\geq 1\% \cdot \text{K}^{-1}$	This work

## References

1. G. Kresse and J. Furthmüller, Efficiency of Ab-initio Total Energy Calculations for Metals and Semiconductors Using A Plane-Wave Basis Set, *Comput. Mater. Sci.*, 1996, **6**, 15-50.
2. (a) E. Francisco, J. Recio, M. Blanco, A. M. Pendás and A. Costales, Quantum-Mechanical Study of Thermodynamic and Bonding Properties of MgF<sub>2</sub>, *J. Phys. Chem. A*, 1998, **102**, 1595-1601; (b) J. Brgoch, S. P. DenBaars and R. Seshadri, Proxies from Ab Initio Calculations for Screening Efficient Ce<sup>3+</sup> Phosphor Hosts, *J. Phys. Chem. C*, 2013, **117**, 17955-17959.
3. (a) R. Hill, The Elastic Behaviour of A Crystalline Aggregate, *Proc. Phys. Soc. London, Sect. A*, 1952, **65**, 349; (b) Z. Wang, B. Shen, F. Dong, S. Wang and W.-S. Su, A First-Principles Study of the Electronic Structure and Mechanical and Optical Properties of CaAlSiN<sub>3</sub>, *Phys. Chem. Chem. Phys.*, 2015, **17**, 15065-15070; (c) Z.-j. Wu, E.-j. Zhao, H.-p. Xiang, X.-f. Hao, X.-j. Liu and J. Meng, Crystal Structures and

Elastic Properties of Superhard IrN<sub>2</sub> and IrN<sub>3</sub> from First Principles, *Phys. Rev. B: Condens. Matter*, 2007, **76**, 054115.

4. (a) G. Henkelman, B. P. Uberuaga and H. Jónsson, A climbing Image Nudged Elastic Band Method for Finding Saddle Points and Minimum Energy Paths, *J. Chem. Phys.*, 2000, **113**, 9901-9904; (b) G. Henkelman and H. Jónsson, Improved Tangent Estimate in the Nudged Elastic Band Method for finding Minimum Energy Paths and Saddle Points, *J. Chem. Phys.*, 2000, **113**, 9978-9985.

5. (a) H. Chen and S. Adams, Bond Softness Sensitive Bond-Valence Parameters for Crystal Structure Plausibility Tests, *IUCrJ*, 2017, **4**, 614-625; (b) H. Chen, L. L. Wong and S. Adams, SoftBV - A Software Tool for Screening the Materials Genome of Inorganic Fast Ion Conductors, *Acta Crystallogr., Sect. B: Struct. Sci.*, 2019, **75**, 18-33; (c) L. L. Wong, K. C. Phuah, R. Dai, H. Chen, W. S. Chew and S. Adams, Bond Valence Pathway Analyzer—An Automatic Rapid Screening Tool for Fast Ion Conductors within softBV, *Chem. Mater.*, 2021, **33**, 625-641.

6. H. Zhang, Z. Gao, G. Li, Y. Zhu, S. Liu, K. Li, Y. Liang, A Ratiometric Optical Thermometer with Multi-Color Emission and High Sensitivity Based on Double Perovskite LaMg<sub>0.402</sub>Nb<sub>0.598</sub>O<sub>3</sub>:Pr<sup>3+</sup> Thermochromic Phosphors, *Chem. Eng. J.*, 2020, **380**, 122491.

7. W. Ran, H. M. Noh, S. H. Park, B. R. Lee, J. H. Kim, J. H. Jeong, J. Shi, Er<sup>3+</sup>-Activated NaLaMgWO<sub>6</sub> Double Perovskite Phosphors and Their Bifunctional Application in Solid-State Lighting and Non-Contact Optical Thermometry, *Dalton Trans.*, 2019, **48**, 4405-4412.

8. M. Runowski, P. Woźny, I. R. Martín, V. Lavín, S. Lisa, Praseodymium Doped YF<sub>3</sub>:Pr<sup>3+</sup> Nanoparticles As Optical Thermometer Based on Luminescence Intensity Ratio (LIR) - Studies in Visible and NIR Range, *J. Lumin.*, 2019, **214**, 116571.
9. M. Jia, G. Liu, Z. Sun, Z. Fu, W. Xu, Investigation on Two Forms of Temperature-Sensing Parameters for Fluorescence Intensity Ratio Thermometry Based on Thermal Coupled Theory, *Inorg. Chem.*, 2018, **57**, 1213-1219.
10. S. Wang, J. Zhang, Z. Ye, H. Yu and H. Zhang, Exploiting Novel Optical Thermometry Near Room Temperature with A Combination of Phase-Change Host and Luminescent Pr<sup>3+</sup> Ion, *Chem. Eng. J.*, 2021, **414**, 128884.

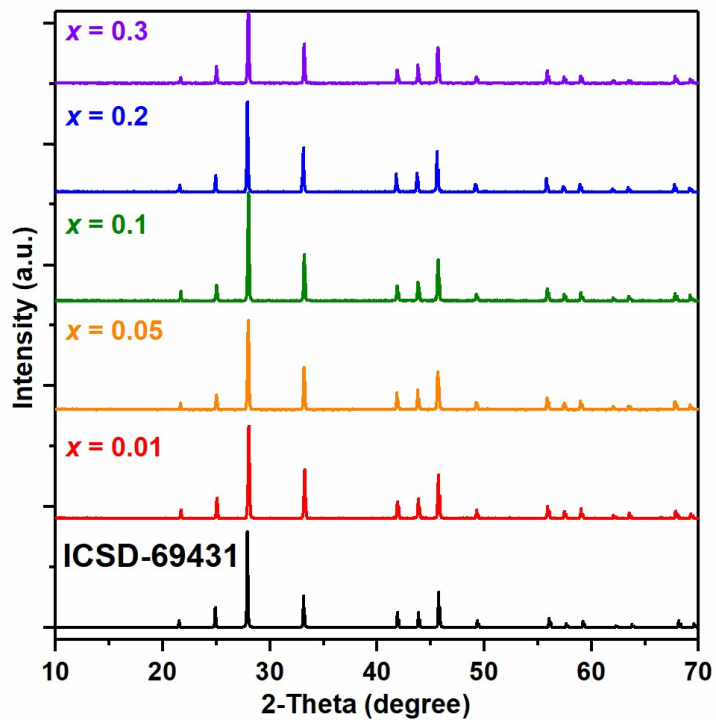


**Fig. S1** XRD patterns of  $\text{Sr}_{2.99-x}\text{Eu}_{0.01}\text{La}_{1+x}\text{P}_{3-x}\text{Si}_x\text{O}_{12}$  ( $x = 0.01, 0.05, 0.10, 0.20$  and  $0.30$ ) phosphors.

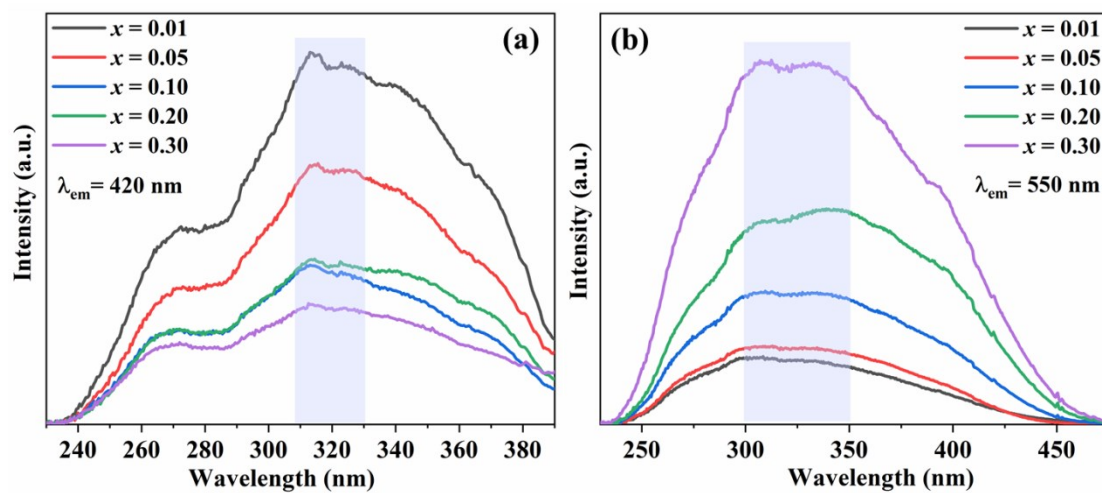


**Fig. S2** Excitation spectra of  $\text{Sr}_{2.99-x}\text{Eu}_{0.01}\text{La}_{1+x}\text{P}_{3-x}\text{Si}_x\text{O}_{12}$  phosphors monitored at (a) 420 nm and (b) 550 nm.

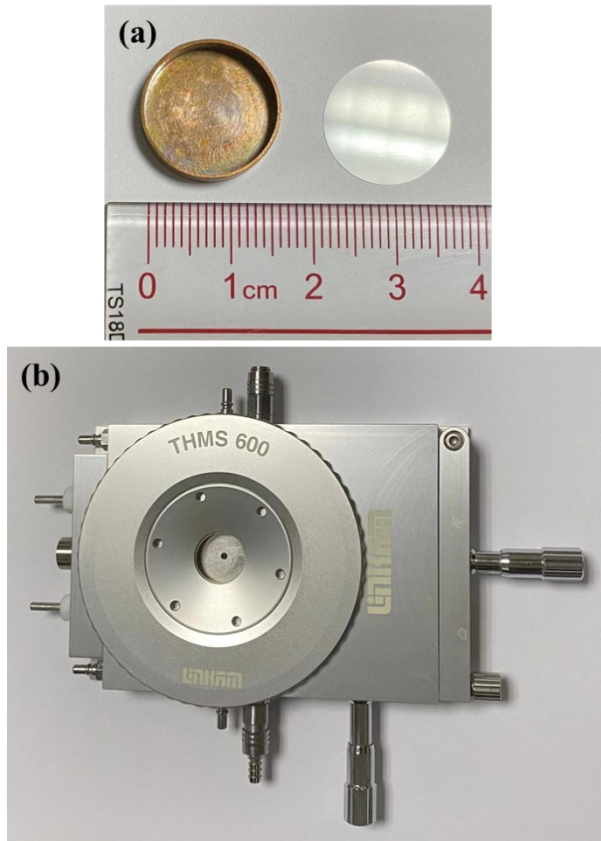


**Fig. S3** Photographs of (a) circular sample groove with glass sheet and (b) a Linkam THMS600 temperature control stage.

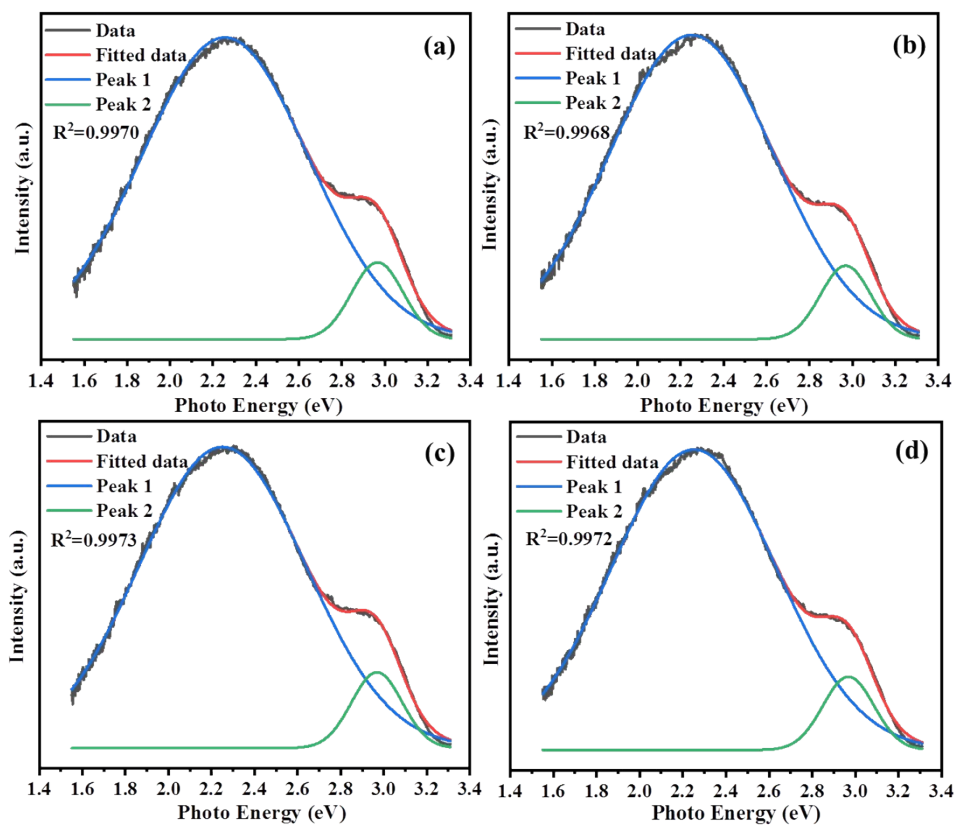


**Fig. S4** The Gaussian fitting for four cycles of emission spectra for  $\text{Sr}_{2.99-x}\text{Eu}_{0.01}\text{La}_{1+x}\text{P}_{3-x}\text{Si}_x\text{O}_{12}$  ( $x = 0.30$ ) phosphor excited at 350 nm with the temperature at 380 K.

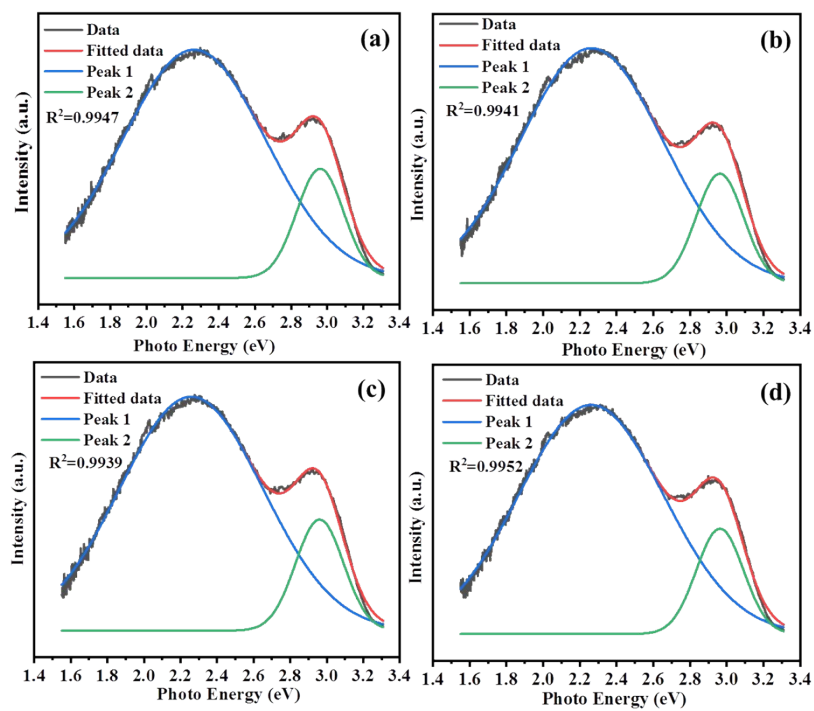


**Fig. S5** The Gaussian fitting for four cycles of emission spectra for  $\text{Sr}_{2.99-x}\text{Eu}_{0.01}\text{La}_{1+x}\text{P}_{3-x}\text{Si}_x\text{O}_{12}$  ( $x = 0.30$ ) phosphor excited at 350 nm with the temperature at 420 K.

The 12 Sr<sup>2+</sup> and 4 La<sup>3+</sup> ions are distributed in 16 metal sites of the unit cell for DFT calculation (Figure S6(a)). There are 1820 possible combinations by the combinatorics and exhaustive method. The huge number makes all the calculation unrealistic. 4 metal sites are in the volume diagonal (green spheres in Figure S6(b)) and the other 12 ones are in 4 layers paralleling with (111) plane (black, red, orange and yellow spheres in Figure S6(c)). Therefore, we simplified the model by the following design: (1) The La<sup>3+</sup> are placed in each layer; (2) The La<sup>3+</sup>-La<sup>3+</sup> distances are kept as long as possible to minimize the electrostatic repulsion as depicted in Figure S6(c).

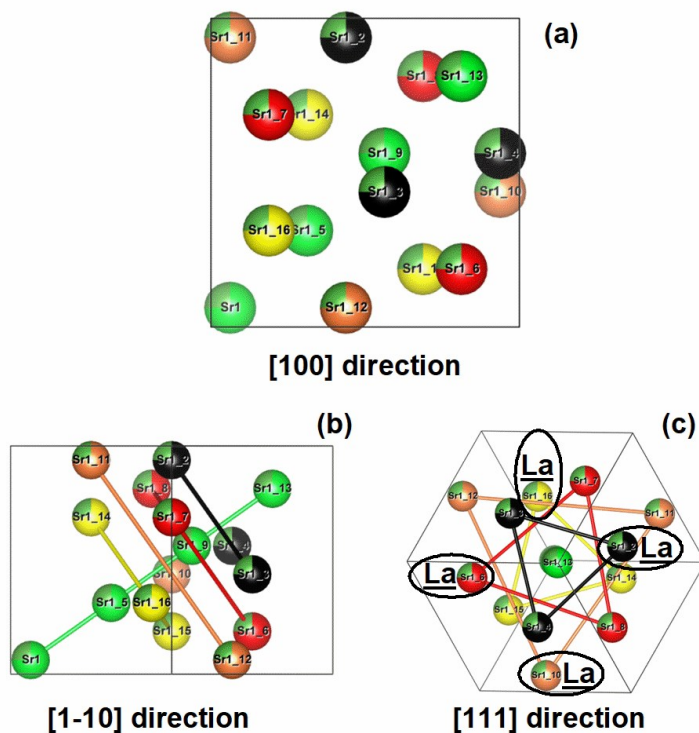


**Fig. S6** Metal sites of Sr<sub>3</sub>La(PO<sub>4</sub>)<sub>3</sub> in (a) [100], (b) [1-10], (c) [111] direction view.